

Article

Experimental Study on Permeability Characteristics of Mudstone under High Temperature Overburden Condition

Jian Ma ¹, Yunlong Zhang ¹, Jiakun Lv ^{1,2,3,*} and Kun Yu ^{2,3} 

¹ College of Architecture and Civil Engineering, Jiangsu University of Science and Technology, Zhenjiang 212000, China; mj198004@mail.ustc.edu.cn (J.M.); m15514340672@163.com (Y.Z.)

² State Laboratory of Coal Resources and Safe Mining, China University of Mining and Technology, Xuzhou 221116, China; yukun@cumt.edu.cn

³ School of Mines, China University of Mining and Technology, Xuzhou 221116, China

* Correspondence: jiakun_l11b4@cumt.edu.cn

Abstract: High-temperature treatment significantly impacts the permeability of mudstone. The permeability of mudstone after exposure to high temperatures is closely influenced by the temperature it experiences and the stress state it is subjected to. This study examines the change in macroscopic physico-mechanical properties of mudstone with temperature following high-temperature treatment. Additionally, we conducted experimental research on the gas and water seepage behavior of mudstone specimens from the top of the coal seam of Taiyuan Group–Shanxi Group in the Ordos Basin. The coal-rock mechanics-permeability test system TAWD-2000 was employed for this purpose. Subsequently, we analyzed the evolution of mudstone permeability after high-temperature treatment with consideration to temperature, axial pressure, and other influencing factors. The findings reveal that gas permeability of mudstone gradually increases with increasing temperature, while water permeability initially decreases and subsequently increases. Furthermore, both gas and water permeability of mudstone exhibit a trend of decreasing and then increasing with rising stress levels after undergoing the same high-temperature treatment. We constructed a quadratic mathematical model with a goodness of fit of 99.4% and 89.2% to describe the relationship between temperature–stress coupling and mudstone gas and water permeability. This model underscores the significance of temperature–stress coupling on mudstone permeability and provides valuable guidance for numerically calculating the gas–water transport law of peripheral rock in the underground coal gasification process and its practical application in engineering.



Citation: Ma, J.; Zhang, Y.; Lv, J.; Yu, K. Experimental Study on Permeability Characteristics of Mudstone under High Temperature Overburden Condition. *Processes* **2023**, *11*, 2828. <https://doi.org/10.3390/pr11102828>

Received: 29 August 2023
Revised: 14 September 2023
Accepted: 18 September 2023
Published: 25 September 2023



Copyright: © 2023 by the authors. Licensee MDPI, Basel, Switzerland. This article is an open access article distributed under the terms and conditions of the Creative Commons Attribution (CC BY) license (<https://creativecommons.org/licenses/by/4.0/>).

Keywords: mudstone caprock; permeation rate; underground coal gasification; fluid–solid–heat coupling

1. Introduction

Underground coal gasification technology is a comprehensive and environmentally friendly method for utilizing coal resources. It involves the in situ conversion of underground coal into combustible gas through thermochemical reactions. During the process of underground coal gasification, a key scientific concern revolves around the evolution of permeability in the surrounding rock under conditions of high temperature and stress. This is crucial for preventing gas leaks or spills to the surface. The study of mudstone permeability characteristics under high-temperature overburden conditions holds great significance in ensuring the stability and safety of underground coal gasification operations.

With the rapid advancement of human exploration in the deep earth, particularly in the area of underground coal gasification, there has been significant interest in understanding the evolution of permeability characteristics of rocks following high-temperature treatment [1–4]. Saik et al. [5] established a heat transfer model for underground coal gasification based on the Newton Raphson method. This model will reveal the relationship between thermal conductivity, specific heat capacity, and the calorific value of bulk density

meters. A method has been developed to determine the placement length of the phase transition boundary of a “generator gas—coal” heterogeneous system and its relationship between the time and temperature of gasification process. This makes it possible to predict in the future the change in the active zones of the underground gas generator along the length of the gas column. Based on this, many scholars have conducted research on the permeability of high-temperature rocks, the permeability of rock is primarily determined by its internal structure, stress state, temperature, and other factors [6,7]. Numerous scholars, both domestically and internationally, have conducted a series of experimental studies and explorations on the permeability characteristics of rocks following high-temperature treatment. Liang et al. [8] investigated the influence of temperature on rock permeability from both theoretical and experimental perspectives. They concluded that there is a positive exponential relationship between rock permeability and temperature after reaching high temperatures (B.L.). Avanthi Isaka et al. [9] utilized CT scanning technology to reconstruct a granite model and conducted a comprehensive investigation into the microstructure changes of granite after exposure to high temperatures. Chen et al. [10] used the electron microscope scanning technique to study the internal fissure development law of granite after high temperature, and proposed that 573 °C (quartz phase transition) is the inflection point of the qualitative change in the number of fissures in granite, and at the same time processing the specimen’s temperature of the increase in the time of the peak stress is gradually reduced. S. Chaki et al. [11] investigated the microscopic characteristics of a rock mass after exposure to high temperatures and found that thermal damage leads to changes in the internal microstructure. These changes, in turn, affect the permeability characteristics of the rock. Jiang et al. [12,13] studied the permeability characteristics of rocks after high temperatures and developed a mathematical model to describe the relationship between permeability and porosity. The aforementioned scholars individually investigated the evolution of the internal structure and fracture of rock after exposure to high temperatures. They examined various factors such as permeability, microstructure using CT and electron microscope scanning, and porosity. Ali LAKIROUHANI et al. [14] investigated the microstructural characteristics and physico-mechanical properties of dolomite at different grain size scales, and demonstrated that there is a strong correlation between microscopic grain size scales and macroscopic physico-mechanical properties. Zhang et al. [12] conducted a study on the pore structure of shale under thermal coupling. They also examined the relationship between permeability and pore pressure and effective stress, and analyzed the conditions under which gas slip affects permeability. Gao et al. [15] studied the effect of temperature and circumferential pressure on the permeability of granite after high temperature, and the results showed that the permeability of granite is mainly affected by temperature and pressure; Hu et al. [16,17] investigated the permeability evolution law of post-high-temperature rocks under different stress conditions based on different engineering backgrounds.

Although there have been numerous studies on the gas permeability characteristics of rocks after exposure to high temperatures and their influential mechanisms, limited research has been conducted on the permeability of liquids in rocks under similar conditions, particularly in high-temperature mudstone [18–24]. Samples of mudstone were collected from the coal bed roof’s aquifer layer in the Taiyuan-Shanxi Formation of the Ordos Basin. These samples underwent high-temperature pretreatment as part of the Underground Coal Gasification (UCG) engineering project, and the resulting changes in mudstone micromorphology were analyzed in response to thermal effects. Building upon this foundation, this study comprehensively analyzes the permeability characteristics of mudstone after exposure to high temperatures and examines the correlation between mudstone permeability, temperature, and stress. The research enriches and advances the field of high-temperature rock mechanics, providing a fundamental basis for numerical simulations and UCG engineering practices.

2. Overview of the Test

2.1. Preparation of Rock Samples and Specimens

The mudstone samples utilized in this test were obtained from the upper water separator of the coal beds in the Taiyuan Group-Shanxi Group formation within the Ordos Basin. X-ray diffraction (XRD) analysis revealed that the primary mineral compositions included 47.6% quartz, 15.8% potassium feldspar, 11.7% plagioclase feldspar, and 24.9% clay minerals. The density of the mudstone samples was determined to be 2125 kg/m³. Following internationally recognized rock mechanics standards, the specimens were prepared as standard cylindrical samples with dimensions of $\Phi 50 \text{ mm} \times 100 \text{ mm}$. Core drilling rigs, rock cutters, and end cutters, as depicted in Figure 1, were employed in the preparation process. Subsequently, the specimens were divided into five groups, with each group containing three specimens. One group served as the control group at ambient temperature, without undergoing any treatment.



Figure 1. Processed rock sample.

2.2. Test Equipment and Principle

The mass of the specimen was determined using an electronic scale with an accuracy of 0.01 g. Additionally, the height and diameter were measured using vernier calipers with an accuracy of 0.02 mm. The heat treatment was conducted in an MXQ1700 type programmable temperature-controlled heating chamber atmosphere furnace. This furnace has a temperature control accuracy of $\pm 1 \text{ }^\circ\text{C}$ and can reach a maximum heating temperature of 1700 $^\circ\text{C}$. Permeability measurements were performed using the Smart perm III flow meter. These tests were carried out at the Coal Rock Mechanics-Seepage Test System (TAWD-2000) located at China University of Mining and Technology (CUMT). Nitrogen and water served as the working mediums. The maximum working pressures for the enclosure and injection were both 70 MPa, whereas the maximum working pressure for axial pressure was 800 MPa. The pressure fluctuation remained within 0.5% over a 48 h period. The permeability of the coal rock was measured using the test machine. The mudstone permeability measurement test is depicted in Figure 2. The equations for calculating permeability for gas and water seepage are as follows, respectively:

$$K_G = \frac{2P_0 Q_G \mu_G L}{A(P_1^2 - P_2^2)} \quad (1)$$

$$K_W = \frac{Q_W \mu_W L}{A(P_1' - P_2')} \quad (2)$$

where: K_G , K_W for mudstone gas, water permeability, mDarcy; Q_G for the standard gas transient flow rate, SmL/s; Q_W for the water flow rate, SmL/s; μ_G for the gas kinetic viscosity, MPa·s; μ_W for the viscosity of water, MPa·s; L for the height of the specimen, cm;

A for the specimen seepage cross-sectional area, cm^2 ; P_0 for the standard atmosphere, MPa; P_1 for the injection pressure, MPa, P_2 for the outgoing pressure, MPa; P'_1 for the injection pressure, MPa, P'_2 for the outgoing pressure, MPa.

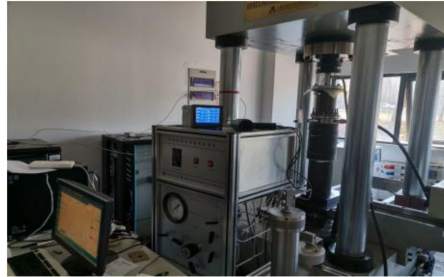


Figure 2. Mudstone permeability measurement test.

2.3. Test Procedure

The control targets for the perimeter pressure of the test were set at 8 MPa, with air or water pressure set at 2 MPa, and temperatures ranging from room temperature to 600 °C (specifically, 200 °C and 400 °C were included). The mudstone's axial pressure was initially loaded to attain the target perimeter pressure value of 8 MPa. Once stabilized, it was further increased to 10 MPa, and subsequently loaded with a gradient of 5 MPa. In practice, slight deviations may occur in some targets due to the instability of gas and water flow, as well as the hysteresis of temperature changes. For more detailed information, please refer to the test results. The specific steps of the test are as follows:

- (1) Heat treatment: The specimen was placed into the muffle furnace, and the mouth was sealed with asbestos. The furnace door was closed, and the heating rate was set at 10 °C/min. The specimens were heated sequentially at temperatures of 20 °C (room temperature), 200 °C, 400 °C, and 600 °C. For each temperature gradient, three specimens were selected, and a constant temperature time of two hours was set. After the heating process is complete, and the muffle furnace has automatically cooled down to 50 °C, the furnace can be opened to remove the specimen, as depicted in Figure 3.

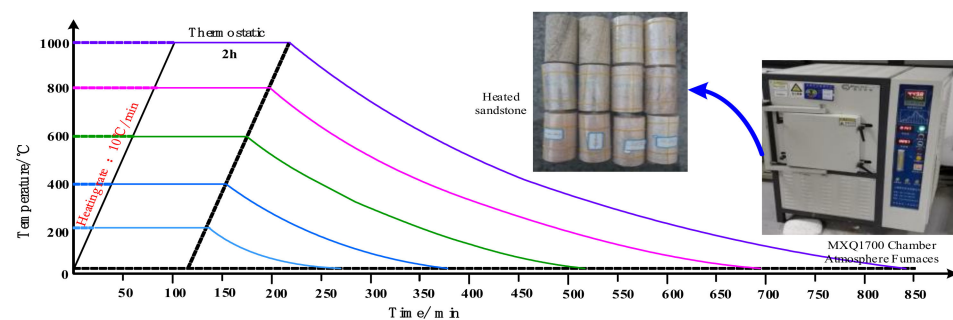


Figure 3. Mudstone specimen heating curve.

- (2) Physical measurements are conducted on the heated specimen, which is sealed after the measurements are taken. The sealed specimen is then positioned in a pressure chamber, which is subsequently placed on the platform of the testing machine. The pressure chamber is connected to both the circumferential pressure line and the gas (or liquid) line.
- (3) Commence the testing machine and set the axial loading rate to 0.02 mm/s, with a target value of 8 MPa. Once the axial pressure reaches the target value, open the pressure loading device and adjust the pressure to 8 MPa.
- (4) Gas permeation test: Open the gas cylinder and regulate the gas injection pressure to a constant 2 MPa using the regulator. Then, open the gas relief valve located at the

outlet of the pressure chamber. After the meter has stabilized, note the transient flow rate value. This value will be used to calculate the gas permeability of the mudstone specimen under this load.

Water Penetration Test: Use the gas cylinder to release gas into the water storage tank at a constant pressure of 2 MPa. Open the valve at the outlet of the water storage tank and wait for water to be discharged from the outlet of the pressure chamber. Then, use a stopwatch to measure the mass of water discharged from the pressure chamber every 30 min. These data will be utilized to calculate the permeability of the specimen under this load.

- (5) Apply an initial axial pressure of 10 MPa. Gradually increase the axial pressure to the next target value using a loading gradient of 5 MPa. Repeat step (4) until the specimen is destroyed (Table 1).

Table 1. Physical parameters of rock samples.

Rock Temperature	Number	Calibre/mm	Heights/mm	Mass/g		Porosity/%
				Before Heating	After Heating	
Ordinary temperatures	NG1-1	49.78	99.97	537.3	537.3	2.58
	NG1-2	49.64	100.17	529.7	529.7	2.58
	NG1-3	49.86	99.95	537.2	537.2	3.30
200 °C	NG2-1	49.73	99.82	529.4	519.8	4.39
	NG2-2	49.79	100.16	530.3	520.4	4.34
	NG2-3	50.19	99.83	536.1	523	4.34
400 °C	NG3-1	50.03	99.96	531.7	502.8	6.31
	NG3-2	49.75	100.12	529.5	500.6	6.52
	NG3-3	49.79	99.99	532.8	507.8	6.88
600 °C	NG4-1	49.72	100.30	532.9	495.2	7.24
	NG4-2	49.93	100.18	531.3	493.5	7.45
	NG4-3	50.24	99.70	529.7	491.3	7.81

3. Analysis of the Variation Rule of Mudstone Macroscopic Physical Properties with Temperature

3.1. Macrophysical Characterization of Mudstone after High Temperature

The mudstone rock, when at room temperature, exhibits a consistent, muddy gray color with no visible surface fissures. Figure 4 depicts the appearance and morphology of the mudstone after being subjected to high temperatures. Furthermore, Figure 5 showcases the temperature-dependent change curve of the mudstone's physical properties, such as the mass loss rate, elongation, and thermal expansion coefficient. These properties were determined through experimental testing.

As depicted in Figure 5, when exposed to temperatures within the range of 600 °C, the specimen undergoes uniform expansion due to heat. Moreover, the mudstone exhibits a mass loss rate and elongation rate that are approximately proportional to the temperature. Within this temperature range, the mineral particles within the mudstone display varying coefficients of thermal expansion based on the thermal expansion coefficient and temperature relationship curve. Consequently, the deformation of the mineral particles is not synchronized after heating. When the thermal stresses between the mineral particles exceed the adhesion, numerous microcracks form within the mudstone, resulting in an increase in specimen elongation. Throughout the heating process, the water associated with the mudstone specimen, including zeolite water, crystallization water, and structural water, are successively released. This leads to a decline in the quality of the specimen.



Figure 4. Appearance and morphology of mudstone after high temperature.

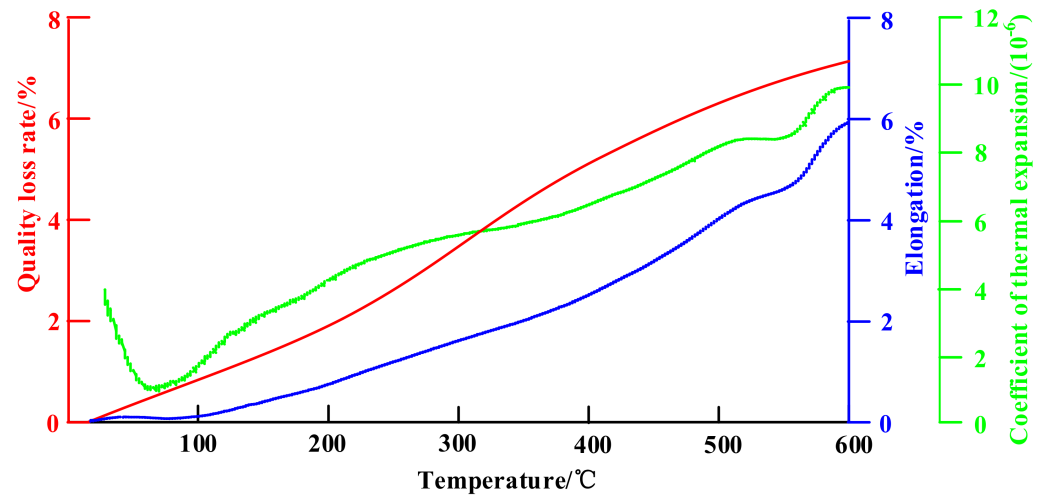


Figure 5. Curve of physical properties of mudstone versus temperature after high temperature.

3.2. Analysis of Microstructural Changes in Mudstone after High Temperature

SEM was used to observe and analyze the internal fine structure of the mudstone after high temperature, as shown in Figure 6, with a magnification of 100–6000 times. Under the action of room temperature, mudstone is dense, there are microporous, irregular shape, microporous size distribution is not uniform, mudstone mineral particles have blocky, flaky, particles rounding degree is good, some particles are even completely rounded to be rounded. The minerals that make up a rock can be predominantly in face-to-face contact, with tiny detrital mineral particles filling in between the larger particles and acting as cementation. The mudstone at 200 °C has a compact structure, with undeveloped pores and cracks, and it is difficult to find larger pores in the test, with good contact between mineral particles. Air holes of different depths and sizes were found on the surface of the mineral particles, which were generally round, partly elliptical or oblate. At 400 °C, under the mudstone surface rock debris began to increase pore size, there are traces of ablation scores (filler between the mineral particles to reduce), the structure is tight, pore cracks are not developed, it is difficult to find a large pore in the test, and the mineral particles between the contact are good. At 600 °C, obvious cracks appeared on the surface of the

sample, the pores further increased, the ablation traces became more obvious, the number of rock debris decreased, the inter-mineral filler was basically ablated, and the mineral particles were bare, and the surface of the sample was in the form of grooves in the high magnification image. More spore-like structures can be found on the mineral surface under high magnification images.

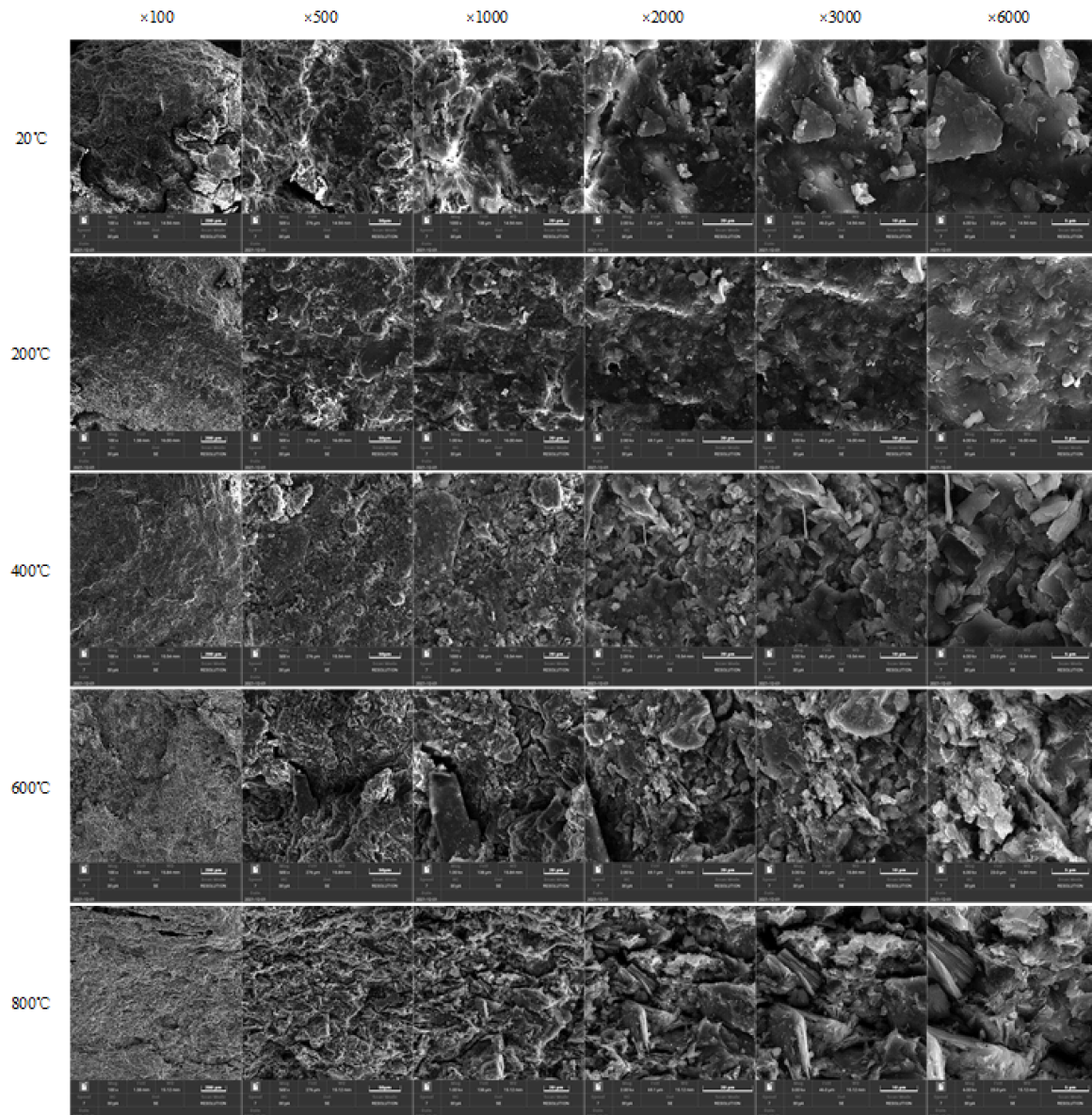


Figure 6. Electron microscope scans of different high-temperature mudstones after natural cooling.

4. Evolutionary Pattern of Mudstone Permeability after High Temperature

4.1. Evolutionary Pattern of Gas Permeability in Mudstone after High Temperature

4.1.1. Changing Law of Gas Permeability of Mudstone under the Condition of Temperature Change

Under initial stress conditions, with an axial pressure and peripheral pressure set at 8 MPa, Figure 7 illustrates the gas permeability evolution of mudstone with temperature. When the temperature increases from ambient to 200 °C, the mudstone's gas permeability rises from 0.089 mDarcy to 0.134 mDarcy, representing a 50.6% increase. Subsequently, as the temperature continues to rise beyond 200 °C, the gas permeability of the mudstone increases rapidly. At temperatures of 400 °C and 600 °C, the gas permeability of the mudstone reaches 0.166 mDarcy and 0.191 mDarcy, respectively. Compared to the

mudstone in its ambient state, these increases amount to 86.5% and 114.6%, respectively. Upon analyzing the reasons for the permeability evolution with temperature, it is observed that the permeability gradually increases between 20–200 °C. This is attributed to the loss of water within the mudstone, resulting in an increase in pore volume. At temperatures ranging from 200–600 °C, the elevated temperature induces continuous thermal damage within the mudstone, leading to crack formation and further augmentation of permeability.

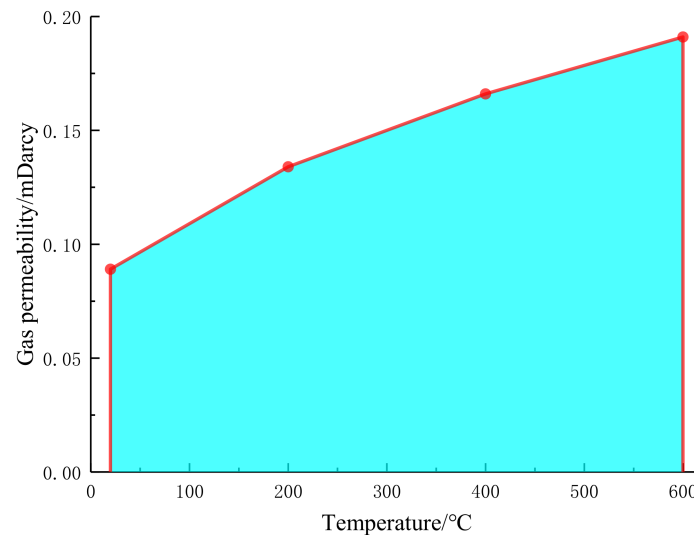


Figure 7. Variation curves of mudstone gas permeability with temperature.

4.1.2. Changing Law of Mudstone Gas Permeability under Stress Change Condition

Keeping the circumferential pressure constant at 8 MPa, the axial pressure was gradually increased from 8 MPa under axial loading conditions, as shown in Figure 8. The strength of mudstone is less than 35 MPa after heat treatment at 200 °C and less than 30 MPa after heat treatment at 400–600 °C. Prior to specimen destruction, the gas permeability of the specimen remained essentially constant or slightly increased as the axial pressure increased across the temperature gradient. For example, the permeability of mudstone specimens heat-treated at 200 °C under axial pressures of 10 MPa, 20 MPa, and 30 MPa was 0.140 mDarcy, 0.134 mDarcy, and 0.242 mDarcy, respectively. The permeability of mudstone specimens heat-treated at 400 °C under axial pressures of 10 MPa, 20 MPa, and 25 MPa was 0.166 mDarcy, 0.159 mDarcy, and 0.236 mDarcy, respectively. The permeability of mudstone specimens heat-treated at 600 °C under axial pressures of 10 MPa, 20 MPa, and 25 MPa was 0.185 mDarcy, 0.185 mDarcy, and 0.306 mDarcy, respectively. The gas permeability of the mudstone remained essentially unchanged across the temperature gradient prior to the destruction of the specimens. The analysis suggests that the pores in the mudstone become compacted after undergoing heat treatment at various temperatures while under initial stress conditions. And when the rock is undergoing rapid damage due to the development of fissures, it can lead to a significant increase in permeability.

4.2. Evolution of Water Permeability in Mudstone after High Temperature

4.2.1. Changing Law of Water Permeability of Mudstone under the Condition of Temperature Change

Under the initial stress conditions (with an axial pressure of 8 MPa and peripheral pressure of 8 MPa), Figure 9 demonstrates the water permeability evolution pattern of the mudstone with temperature. When the temperature was increased from ambient to 200 °C, the water permeability of the mudstone decreased from 0.0182 mDarcy to 0.0140 mDarcy, indicating a 23.1% decrease. Subsequently, as the temperature continued to rise above 200 °C, the water permeability of the mudstone increased rapidly. At temperatures of 400 °C and 600 °C, the water permeability of the mudstone reached 0.0437 mDarcy and 0.0739 mDarcy, respectively. These values represent reductions of 140.1% and 306.0%

compared to the water permeability of the mudstone at room temperature. Analyzing the reasons for the permeability evolution with temperature, the following trends can be observed: temperatures ranging from 20–200 °C result in the thermal expansion of the mudstone, which leads to the compaction of larger pores and a consequent decrease in water permeability. On the other hand, temperatures between 200–600 °C cause the thermal degradation of the rock, leading to the formation of cracks and a rapid increase in water permeability.

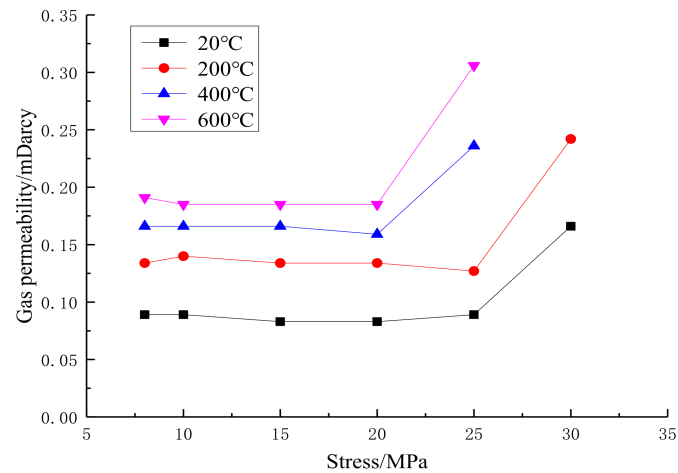


Figure 8. Variation curve of permeability of mudstone gas with axial pressure at different temperatures.

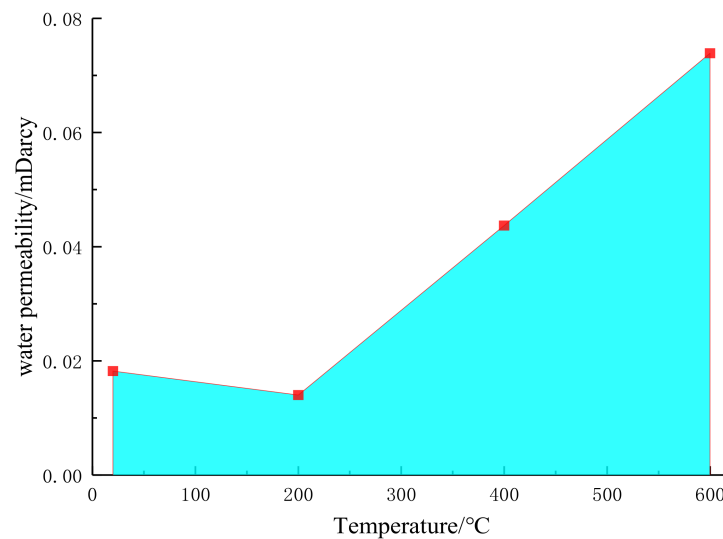


Figure 9. Variation curves of mudstone water permeability with temperature.

4.2.2. Changing Law of Mudstone Water Permeability under Stress Change Condition

Keeping the circumferential pressure constant at 8 MPa, the axial pressure was gradually increased from 8 MPa under axial loading conditions, as shown in Figure 10. The strength of mudstone is less than 30 MPa after heat treatment at 200 °C and less than 25 MPa after heat treatment at 400–600 °C. Revised 2: The permeability of the mudstone specimens, which were heat-treated at 200 °C, at axial pressures of 10 MPa, 20 MPa, and 25 MPa, were 0.0137 mDarcy, 0.0286 mDarcy, and 0.0580 mDarcy, respectively. Similarly, the permeability of the mudstone specimens, heat-treated at 400 °C, at axial pressures of 10 MPa, 15 MPa, and 20 MPa, were 0.0393 mDarcy, 0.0543 mDarcy, and 0.1170 mDarcy, respectively. Finally, the permeability of the mudstone specimens, heat-treated at 600 °C, at axial pressures of 10 MPa, 15 MPa, and 20 MPa, were 0.0659 mDarcy, 0.0749 mDarcy,

and 0.1720 mDarcy, respectively. Reason 2: The original text lacked clarity and readability due to the repetitive structure and lack of proper sentence structure. The revised version separates the information into clear and concise sentences, making it easier to understand the different heat treatment conditions and their corresponding permeability values. With the increase in axial pressure, similar to the change in mudstone gas permeability, the water permeability of the specimen at each temperature gradient remains basically unchanged or slightly increases before the specimen is destroyed. This is because there is a lack of large penetrating fissures. However, when the rock is rapidly destroyed, the permeability of the rock drastically increases due to the creation of large penetrating fissures.

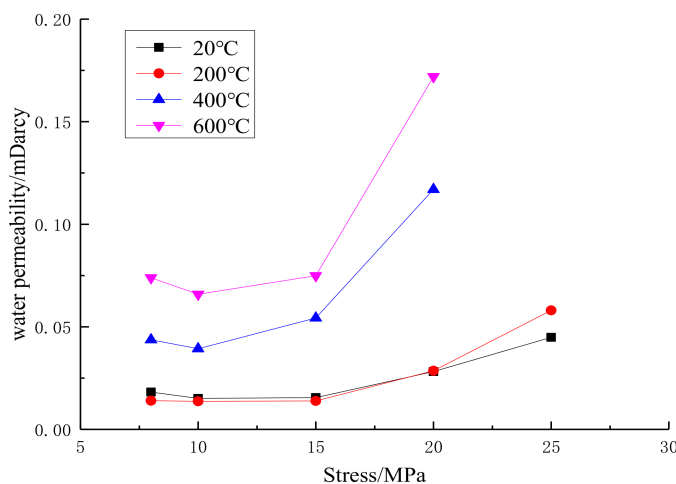


Figure 10. Variation curves of mudstone water permeability with axial pressure at different temperatures.

4.3. Mathematical Modeling of the Relationship between Temperature–Stress and Mudstone Permeability

Gas Permeability–Temperature–Stress Model

According to the results of this test, the aim was to analyze the relationship between the permeability of mudstone to gas and water and the changes in temperature and stress. Various mathematical models were used to fit the test data, and the comparison showed that higher degree binary polynomials provided a better fit. The equation fitted for the permeability of mudstone to gas and water as a function of temperature and stress is

$$K_G = 8.792 \times 10^{-2} - 5.039 \times 10^{-4}x + 2.925 \times 10^{-4}y + 2.236 \times 10^{-7}xy - 2.035 \times 10^{-7}y^2 \quad (3)$$

$$K_W = 1.354 \times 10^{-1} - 1.932 \times 10^{-2}x - 1.206 \times 10^{-4}y + 6.799 \times 10^{-4}x^2 + 1.304 \times 10^{-5}xy + 1.548 \times 10^{-7}y^2 \quad (4)$$

where x is the axial pressure, MPa; y is the temperature, °C.

The graphs in Figures 11 and 12, respectively, show the relationship between the permeability of mudstone to gas and water and the variations in temperature and stress during the testing of rock samples. From the mathematical models of two types of mudstone, the relationship between gas and water permeability and axial pressure and temperature under changing temperature–stress conditions can be observed. It is evident that this relationship follows a quadratic function, and the data show a high degree of fit, with R^2 values of 99.4% and 89.2% for gas and water permeability, respectively. The degree of thermal damage to the specimen after high-temperature treatment is closely related to the temperature and stress. The higher the temperature and the greater the stress experienced by the mudstone specimen, the more severe the damage and destruction of the internal structure. This leads to the development of more pores and fissures, resulting in a significant change in permeability. The function fitting results can effectively predict the change of permeability due to temperature–stress during underground coal mining. At the same time, combined

with the results of Saik's [5] study, it can be determined that the relationship between temperature and time in the process of coal underground gasification project, based on which the results of this paper can be linked with the coal underground gasification project, in order to provide the necessary data support for subsequent numerical calculations on the law of gas transport in the peripheral rock of the underground gasification cavity of the coal and the analysis of the stability of the gas transport law.

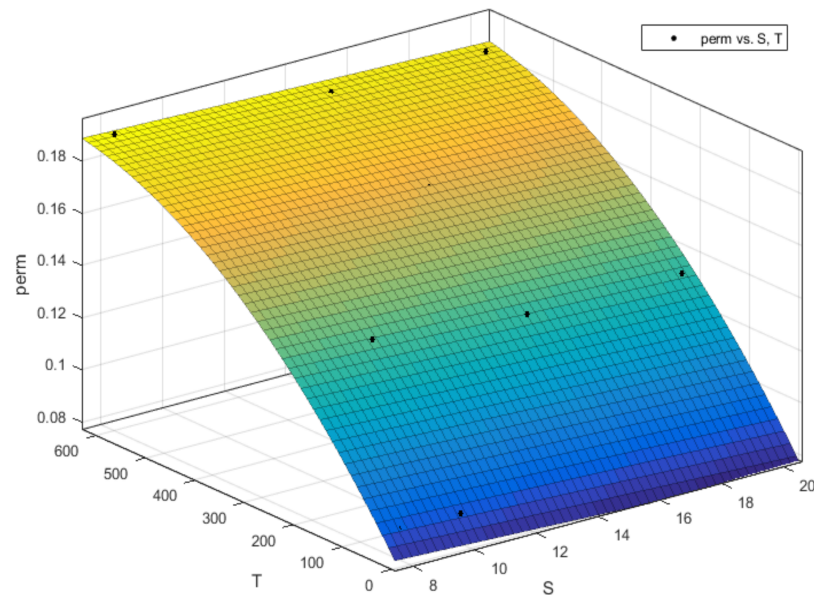


Figure 11. Fitted surfaces for gas permeability of mudstone under temperature–stress coupling.

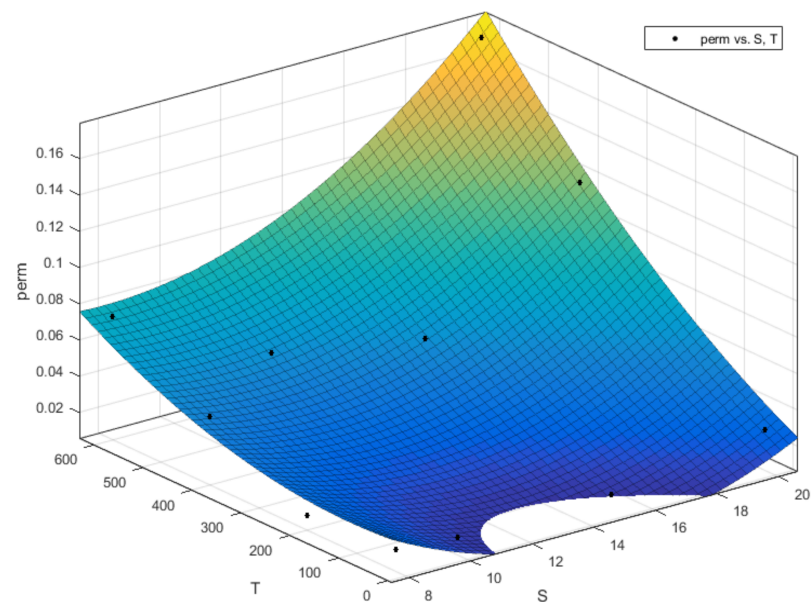


Figure 12. Fitted surfaces for water permeability of mudstone under temperature–stress coupling.

5. Conclusions and Recommendations

Temperature significantly influences the thermophysical properties of mudstone. The rate of mudstone mass loss and elongation generally correlates with temperature. Moreover, the coefficient of thermal expansion of mudstone specimens initially increases and then decreases as temperature rises. Concurrently, temperature also impacts the microstructure of mudstone. When the temperature reaches 400 °C, the mudstone's surface begins to accumulate rock debris, subsequently resulting in an increase in pores and signs of ablation.

At a temperature of 600 °C, the mudstone develops more fissures and pores, and the signs of ablation become more pronounced.

Under initial stress conditions, the permeability of gas in mudstone increases with temperature, albeit at a decreasing rate. However, the permeability of water in mudstone initially decreases and then increases with temperature. Specifically, the water permeability decreases up to 200 °C, but subsequently exhibits a significant increase from 200 °C to 600 °C. Additionally, at a given temperature, the permeability of gas in mudstone tends to decrease initially and then increase with increasing stress.

Quadratic mathematical models were constructed to analyze the changes in gas permeability and water permeability in mudstone under temperature–stress coupling. The models achieved a fit of 99.4% for gas permeability and 89.2% for water permeability. The changes in permeability caused by variations in temperature and stress can be predicted using the fitting function. This function provides the necessary data support for subsequent numerical calculations of the gas–water transport law in the surrounding rock of coal underground gasification cavities, as well as for practical engineering applications.

The high temperatures generated by coal combustion, pyrolysis, and gasification affect the permeability of the overburden rock. The evolution of mudstone permeability establishes a foundational dataset for permeable gasification technology, which is crucial for successful industrial trials.

Author Contributions: J.M.: software, writing original. Y.Z.: conceptualization, methodology. J.L.: supervision, software. K.Y.: funding acquisition. All authors have read and agreed to the published version of the manuscript.

Funding: This work was supported by Suzhou science and technology development plan (SNG2021039, SS202109) and Zhangjiagang science and technology development plan (ZKYY2212). China Postdoctoral Science Foundation (No. 2023T160686).

Data Availability Statement: Not applicable.

Conflicts of Interest: The authors declare no conflict of interest.

References

1. Zhang, Y.L.; Zhang, M.T.; Song, W.Y. Basic equations of channel model for underground coal gasification. *Prog. Nat. Sci.* **2002**, *12*, 364–367.
2. Rezk, M.G.; Foroozesh, J. Study of convective-diffusive flow during CO₂ sequestration in fractured heterogeneous saline aquifers. *J. Nat. Gas Sci. Eng.* **2019**, *69*, 102926. [[CrossRef](#)]
3. Wachowicz, J.; Janoszek, T.; Iwaszenko, S. Model Tests of the Coal Gasification Process. *Arch. Min. Sci.* **2010**, *55*, 249–262.
4. Yang, L.H. Nonlinear coupling mathematical models on percolation-patterned underground coal gasification. *Int. J. Energy Res.* **2005**, *29*, 1331–1353. [[CrossRef](#)]
5. Saik, P.; Berdnyk, M. Mathematical model and methods for solving heat-transfer problem during underground coal gasification. *Min. Miner. Depos.* **2022**, *16*, 87–94. [[CrossRef](#)]
6. Ding, Q.-L.; Ju, F.; Song, S.-B.; Yu, B.-Y.; Ma, D. An experimental study of fractured sandstone permeability after high-temperature treatment under different confining pressures. *J. Nat. Gas Sci. Eng.* **2016**, *34*, 55–63. [[CrossRef](#)]
7. Ding, Q.-L.; Wang, P.; Cheng, Z. Permeability evolution of fractured granite after exposure to different high-temperature treatments. *J. Pet. Sci. Eng.* **2022**, *208*, 109632. [[CrossRef](#)]
8. Bin, L.; Gao, H.; Lan, Y. Theoretical Analysis and Experimental Study on Relation between Rock Permeability and Temperature. *Chin. J. Rock Mech. Eng.* **2005**, *24*, 2009–2012.
9. Isaka, B.L.A.; Ranjith, P.G.; Rathnaweera, T.D.; Perera, M.S.A.; De Silva, V.R.S. Quantification of thermally-induced microcracks in granite using X-ray CT imaging and analysis. *Geothermics* **2019**, *81*, 152–167. [[CrossRef](#)]
10. Chen, S.; Yang, C.; Liu, J.; Wei, X. Evolution of cracks and permeability of granites suffering from different thermal damages. *Chin. J. Geotech. Eng.* **2017**, *39*, 1493–1500.
11. Chaki, S.; Takarli, M.; Agbodjan, W.P. Influence of thermal damage on physical properties of a granite rock: Porosity, permeability and ultrasonic wave evolutions. *Constr. Build. Mater.* **2008**, *22*, 1456–1461. [[CrossRef](#)]
12. Jiang, G.; Zuo, J.; Ma, T.; Wei, X. Experimental Investigation of Wave Velocity-Permeability Model for Granite Subjected to Different Temperature Processing. *Geofluids* **2017**, *2017*, 6586438. [[CrossRef](#)]
13. Jiang, G.; Zuo, J.; Li, L.; Ma, T.; Wei, X. The Evolution of Cracks in Maluanshan Granite Subjected to Different Temperature Processing. *Rock Mech. Rock Eng.* **2018**, *51*, 1683–1695. [[CrossRef](#)]

14. Lakirouhani, A.; Asemi, F.; Zohdi, A.; Medzvieckas, J.; Kliukas, R. Physical parameters, tensile and compressive strength of dolomite rock samples: Influence of grain size. *J. Civ. Eng. Manag.* **2020**, *26*, 789–799. [[CrossRef](#)]
15. Gao, H.; Lan, Y.; Guo, N. Study on Microscopic Pore Structure and Permeability of Granite After Temperature Action. *Mater. Rep.* **2023**, *37*, 131–136.
16. Jin, P.; Hu, Y.; Shao, J.; Zhao, G.; Li, X.; Li, C. Experimental study on physico-mechanical and transport properties of granite subjected to rapid cooling. *Chin. J. Rock Mech. Eng.* **2018**, *37*, 2556–2564. [[CrossRef](#)]
17. Hu, Y.; Zhao, Y.; Yang, D.; Kang, Z. Experimental Study of Effect of Temperature on Permeability Characteristics of Lignite. *Chin. J. Rock Mech. Eng.* **2010**, *29*, 1585–1590.
18. Ge, Z.; Sun, Q.; Li, W. Temperature and Pressure Effect on Permeability of Chinese Sandstone: A Review. *Acta Geodyn. Geomater.* **2018**, *15*, 289–296. [[CrossRef](#)]
19. Liu, W.; Wu, D.; Xu, H.; Chu, X.; Zhao, W.; Yang, Y. A permeability evolution model of coal particle from the perspective of adsorption deformation. *Energy Sci. Eng.* **2021**, *9*, 577–587. [[CrossRef](#)]
20. Chao, Z.; Ma, G.; He, K.; Wang, M. Investigating low-permeability sandstone based on physical experiments and predictive modeling. *Undergr. Space* **2021**, *6*, 364–378. [[CrossRef](#)]
21. Lu, S.; Li, M.; Ma, Y.; Wang, S.; Zhao, W. Permeability changes in mining-damaged coal: A review of mathematical models. *J. Nat. Gas Sci. Eng.* **2022**, *106*, 104739. [[CrossRef](#)]
22. Chen, Z.N.; Feng, Z.J.; Mi, C.; Zhang, C. Real-time permeability evolution of limestone under high temperature and triaxial stresses. *Geomech. Geophys. Geo-Energy Geo-Resour.* **2023**, *9*, 43. [[CrossRef](#)]
23. Tao, M.; Xue, Y.B.; Ma, J.W.; Yang, Y.; Wen, L.; Jing, Z.; Li, E.B. Evolution of permeability and microscopic pore structure of sandstone and its weakening mechanism under coupled thermo-hydro-mechanical environment subjected to real-time high temperature. *Eng. Geol.* **2021**, *280*, 105955. [[CrossRef](#)]
24. Pathiranagei, S.V.; Gratchev, I.; Kong, R. Engineering properties of four different rocks after heat treatment. *Geomech. Geophys. Geo-Energy Geo-Resour.* **2021**, *7*, 16. [[CrossRef](#)]

Disclaimer/Publisher’s Note: The statements, opinions and data contained in all publications are solely those of the individual author(s) and contributor(s) and not of MDPI and/or the editor(s). MDPI and/or the editor(s) disclaim responsibility for any injury to people or property resulting from any ideas, methods, instructions or products referred to in the content.